

# TORQUE IMPROVEMENT OF 3-RRR PLANAR MANIPULATOR ON A SQUARE-SHAPED TRAJECTORY

Soheil S. Parsa<sup>1</sup>, Juan A. Carretero<sup>1</sup>, Roger Boudreau<sup>2</sup>

<sup>1</sup>*Dept. of Mechanical Engineering, University of New Brunswick, Fredericton, NB, CANADA*

<sup>2</sup>*Département de génie mécanique, Université de Moncton, Moncton, NB, CANADA*

*Email: S.Parsa@unb.ca; Juan.Carretero@unb.ca; roger.a.boudreau@umoncton.ca*

---

## ABSTRACT

The actuation of conventionally fixed linkage parameters such as the moment of inertia can enhance the system dynamic performance. Recently, the idea of internal redundancy was introduced which is considered as variation of link geometry and may contribute in some cases to overcome the limits of the robot's actuator. This paper investigates the effects of adding a portable mass to the distal link of the 3-RRR planar manipulator which is allowed to trace a square-shaped trajectory with rounded corners. The proposed method uses the manipulator's dynamic model to actively optimize the location of the redundant masses at every point along the trajectory to improve the dynamic performance of the manipulator while sorting a trajectory with sharp corners. Numerical examples are shown to support the idea.

**Keywords:** internal redundancy; parallel manipulator; dynamic modelling; square-shaped trajectory; optimization.

---

## RÉDUCTION DES COUPLES D'UN MANIPULATEUR 3-RRR PLAN SUIVANT UNE TRAJECTOIRE CARRÉE

### RÉSUMÉ

L'actionnement de paramètres qui sont normalement fixes des membres, tels que le moment d'inertie, peut améliorer la performance dynamique d'un système. La redondance interne a récemment été proposée pour modifier la géométrie des membres et ainsi pallier aux limitations de l'actionneur du robot. Cet article examine les effets de l'addition d'une masse déplaçable sur chaque membre distal d'un manipulateur 3-RRR plan lorsqu'il suit une trajectoire carrée avec des coins arrondis. La méthode proposée utilise le modèle dynamique du manipulateur pour optimiser la position des masses redondantes à chaque point le long de la trajectoire et ainsi améliorer la performance dynamique du manipulateur lorsqu'il suit une trajectoire avec des virages brusques. Des exemples numériques sont présentés.

**Mots-clés :** redondance interne ; manipulateur parallèle ; model dynamique ; trajectoire carrée ; optimisation.

## 1. INTRODUCTION

Parallel manipulators have been widely used in the manufacturing industry where continuous paths have to be followed with high tracking accuracy. These tasks include welding, laser cutting, assembly and deburring, to name a few. Unfortunately, manipulators may suffer from tracking error when the trajectory has a sharp corner. More specifically, when the manipulator approaches a sharp corner, the acceleration changes drastically which requires large torques from the actuators. Consequently, the sharp corner trajectory turns to a rounded corner trajectory since the maximum torque of the actuators is limited. The effects of internal redundancy are investigated here when tracking a sharp corner.

Redundancy in parallel manipulators is normally divided into kinematic redundancy, actuation redundancy and branch redundancy [1–5]. Actuation redundancy consists of replacing passive joints with active ones [2, 6–8] where the number of degrees-of-freedom or mobility of the manipulator does not change. Although actuation redundancy can help either eliminate or reduce singular configurations, issues such as force interference make the manipulators more complex to analyze, design and control [9, 10]. The second type of redundancy is called branch redundancy where an extra actuated branch is added to the manipulator [11]. Branch redundancy can improve the force capabilities of the manipulator and reduce the number of singular configurations. The third type of redundancy is called kinematic redundancy where active joints and links are added to one or more branches of the manipulator [3, 12]. This type of redundancy can enhance the dexterity of the manipulator as well as enlarge its workspace. Additionally, kinematic redundancy allows to follow trajectories choosing configurations that are far from singular configurations since the inverse displacement problem has an infinite number of solutions [13].

Redundant parallel manipulators have been widely used to improve the trajectories of parallel robots. For instance, Cha *et al.* [14] showed that kinematically redundant manipulators can effectively avoid singular configurations thus increasing the singularity-free workspace of the parallel manipulator. Wu *et al.* [15] used a 3-DOF parallel manipulator with actuation redundancy to decrease the tracking error on a trajectory with a rounded corner.

Jouaneh *et al.* [16] presented a new method of path planning for trajectories with sharp corners where the tool (at the end of the manipulator) and workpiece move simultaneously. The path including the sharp corner is divided into two smooth paths. Ruggiu and Carretero [17] applied a kinematically redundant parallel manipulator to minimize the acceleration of the actuators while following certain trajectories. The method was applied on a kinematically redundant parallel manipulator following square paths with rounded corners. They showed that the accelerations of the actuated joints on the kinematically redundant manipulator are significantly less than those needed for a non-redundant manipulator.

Recently, a new type of redundancy called internal redundancy has been the focus of some attention in the context of serial manipulators [18]. Similar to the types of redundancy described earlier, a new set of degrees of freedom (DOF) is added to the serial manipulator. However, in contrast with the redundant actuators and/or links described earlier, the new DOF is used to change the internal geometry of a link resulting in the change of the location of the link's centre of mass and its inertial mass distribution parameters (*i.e.*, its mass moment of inertia). Since the changes are made within the internal members of the link, the redundant DOF does not have a direct effect on the end effector pose (*i.e.*, position and orientation).

In this paper, the concept of internal redundancy is applied to a planar parallel manipulator. First, a 3-RRR manipulator with internal redundancy in all three branches is described and its kinematic and dynamic equations (Sections 2) are derived. Then, an optimization problem is formulated where the displacement of each of the portable masses at every point throughout a trajectory is sought to minimize the torques at the base actuators (Section 3). The architectural parameters and trajectory planning algorithm are explained through a numerical example and are presented in Section 4 and then discussed in more detail in Section 5. Finally, Section 6 presents the conclusions and briefly discusses potential future work.

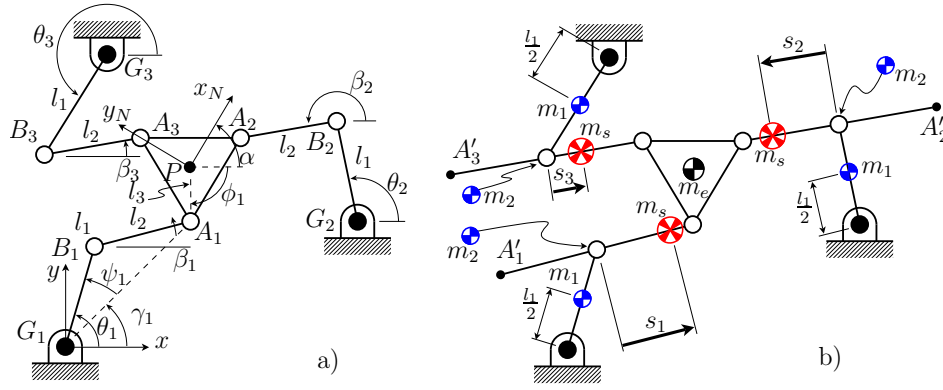


Fig. 1. 3-RRR planar manipulator: a) basic kinematic parameters and b) location of the centre of mass of each component ( $l_i$  are fixed values while  $s_i$  are variable).

## 2. THE 3-RRR MANIPULATOR WITH INTERNAL REDUNDANCY

A 3-DOF planar parallel manipulator shown in Fig. 1a is chosen to investigate the effect of internal redundancy in parallel manipulators. The manipulator is a symmetrical 3-RRR manipulator with base ( $G_1G_2G_3$ ) and end effector ( $A_1A_2A_3$ ) as equilateral triangles. The three revolute actuators to move the manipulator's end effector are located at  $G_i$ , the base joint of each branch. The length of the proximal links, *i.e.*, links  $G_iB_i$  ( $i = 1, 2, 3$ ), is denoted by  $l_1$  while the length of the distal link, *i.e.*,  $B_iA_i$  ( $i = 1, 2, 3$ ) is denoted by  $l_2$ .

In order to study the concept of internal redundancy, a portion of the distal link (the portion from  $B_i$  to  $A'_i$ ) protrudes on the opposite side of the revolute joint at  $B_i$  and creates a linear track from  $A_i$  to  $A'_i$  where the redundant mass  $m_s$  can slide on (see Fig. 1b). The position of the mass relative to the elbow joint  $B_i$  is given by  $s_i$  and is measured in the direction of  $A_i$ . Since the masses  $m_s$  are mounted on tracks or prismatic joints, their position along  $A_iA'_i$  can be actively controlled. More specifically, the distance  $s_i$  from elbow joint  $B_i$  to the centre of mass  $m_s$  can be actively controlled thus changing the overall dynamic properties and effects of links  $A'_iA_i$  [19, 20].

To help complete the dynamic model, each element is given a mass while symmetry is assumed to simplify the analysis. Moreover, the links are modelled as slender rods. The proximal links are all assigned a mass  $m_1$  with their centre of mass located halfway between  $G_i$  and  $B_i$  while all three distal links are assigned a mass  $m_2$  with their centre of mass located halfway between  $A'_i$  and  $A_i$ . The moving platform is assigned a mass  $m_e$  with its barycentre located at the centroid of the moving platform.

### 2.1. Kinematics

The base coordinate frame  $O-xy$  (denoted by  $\{O\}$ ) shown in Fig. 1 is fixed on point  $G_1$ . A moving coordinate frame  $P-x_Ny_N$  (denoted by  $\{N\}$ ) is attached to the barycentre of the moving platform.

The Jacobian matrix of the manipulator is written as follows:

$$\mathbf{J} = \begin{bmatrix} \frac{-a_1}{c_1} & \frac{-b_1}{c_1} & \frac{-d_1}{c_1} \\ \frac{-a_2}{c_2} & \frac{-b_2}{c_2} & \frac{-d_2}{c_2} \\ \frac{-a_3}{c_3} & \frac{-b_3}{c_3} & \frac{-d_3}{c_3} \end{bmatrix} \quad (1)$$

where the elements of this Jacobian matrix can be shown to be [21]:

$$a_i = -h_1(x - x_{G_i}) + h_3 \cos \theta_i + h_1 \cos \phi_i \quad (2)$$

$$b_i = -h_1(y - y_{G_i}) + h_1 \sin \theta_i + h_2 \sin \phi_i \quad (3)$$

$$c_i = h_3[(y - y_{G_i}) \cos \theta_i - (x - x_{G_i}) \sin \theta_i] + \sin(\theta_i - \phi_i) \quad (4)$$

$$d_i = h_2[(y - y_{G_i}) \cos \phi_i - (x - x_{G_i}) \sin \phi_i] - \sin(\theta_i - \phi_i) \quad (5)$$

where  $x_{G_i}$  and  $y_{G_i}$  are the Cartesian components of the position of point  $G_i$  while  $h_1 = \frac{1}{l_1 l_3}$ ,  $h_2 = \frac{1}{l_1}$  and  $h_3 = \frac{1}{l_3}$ . For a given pose, expressions to compute angles  $\theta_i$  and  $\phi_i$ , shown in Fig 1, are given in [20].

## 2.2. Link Jacobian Matrices

Since the Principle of Virtual Work is applied to develop the dynamic model of the 3-RRR manipulator, link Jacobian matrices have to be derived. When the end effector is subjected to a virtual displacement, the link Jacobian sub-matrix related to the linear velocity provides the virtual displacement of a point on a link, while the link Jacobian sub-matrix related to angular velocity produces the virtual angular displacement of a link. Points  $G_i$ ,  $B_i$  and  $P$  are considered as the pivotal points of links  $G_i B_i$ ,  $B_i A_i$  and the moving platform, respectively. The link Jacobian sub-matrix related to the angular velocity of link  $G_i B_i$  is written as follows:

$$\mathbf{G}_{i1} = \begin{bmatrix} \frac{-a_i}{c_i} & \frac{-b_i}{c_i} & \frac{-d_i}{c_i} \end{bmatrix}. \quad (6)$$

The link Jacobian sub-matrix related to the linear velocity of point  $G_i$  is zero since the velocity of that point is zero and is thus written as:

$$\mathbf{H}_{i1} = \mathbf{0} \quad (7)$$

The link Jacobian sub-matrix related to the linear velocity of point  $B_i$  and the link Jacobian sub-matrix related to the angular velocity of link  $B_i A_i$  are written as follows:

$$\mathbf{H}_{i2} = \frac{l_1}{c_i} \begin{bmatrix} a_i \sin \theta_i & b_i \sin \theta_i & d_i \sin \theta_i \\ -a_i \cos \theta_i & -b_i \cos \theta_i & -d_i \cos \theta_i \end{bmatrix} \quad (8)$$

$$\mathbf{G}_{i2} = \begin{bmatrix} \frac{-\sin \beta_i}{l_2} & \frac{\cos \beta_i}{l_2} \end{bmatrix} \left( \begin{bmatrix} \mathbf{e}_1 & \mathbf{e}_2 \end{bmatrix} + \mathbf{N} \mathbf{R} \mathbf{r}_{A_i} \mathbf{e}_3^T - \begin{bmatrix} -l_1 \sin \theta_i \\ l_1 \cos \theta_i \end{bmatrix} \mathbf{G}_{i1} \right) \quad (9)$$

where  $\mathbf{e}_1 = [1 \ 0 \ 0]^T$ ,  $\mathbf{e}_2 = [0 \ 1 \ 0]^T$  and  $\mathbf{e}_3 = [0 \ 0 \ 1]^T$ . Also,  $\beta_i$  describes the angle of link  $B_i A_i$  with respect to the horizontal  $x$  direction. The rotation matrix  $\mathbf{R}$  describes frame  $\{N\}$  relative to frame  $\{O\}$  and  $\mathbf{r}_{A_i}$  is the position vector of point  $A_i$ . The determination of angle  $\beta_i$ , as well as the first and second derivatives of  $\theta_i$  and  $\beta_i$  that will be used later, are developed in [20].

The link Jacobian sub-matrix related to the angular velocity of the moving platform and the link Jacobian sub-matrix related to the linear velocity of point  $P$  are written as follows:

$$\mathbf{G}_N = \mathbf{e}_3^T \quad (10)$$

$$\mathbf{H}_N = \begin{bmatrix} 1 & 0 & 0 \\ 0 & 1 & 0 \end{bmatrix}. \quad (11)$$

## 2.3. Inertial Force and Inertial Moment

Here, the Newton-Euler formulation is applied to develop the inertial forces and the inertial moments of each moving body about its centre of mass. Then, these inertial forces and moments are calculated about

pivotal points (*i.e.*, points  $A_i, B_i$  and  $G_i$ ). The inertial force and moment of link  $G_i B_i$  about pivotal point  $G_i$  are written as follows:

$$\mathbf{F}_{i1} = -m_1 \left( \frac{l_1}{2} \ddot{\theta}_i [-\sin \theta_i \cos \theta_i]^T - \frac{l_1}{2} \dot{\theta}_i^2 [\cos \theta_i \sin \theta_i]^T \right) \quad (12)$$

$$M_{i1} = -\ddot{\theta}_i I_{i1} \quad (13)$$

where  $\theta_i$ ,  $\dot{\theta}_i$  and  $\ddot{\theta}_i$  are the angular displacement, angular velocity and angular acceleration of actuator  $i$ , and  $I_{i1}$  is the moment of inertia of link  $G_i B_i$  about point  $G_i$ .

The influence of internal redundancy appears in the inertial force and moment of the distal links where the moment of inertia and mass centre of the links vary with respect to the position of  $m_s$ . The equations for the inertial force and moment about point  $B_i$  of the distal links are written as follows:

$$\mathbf{F}_{i2} = -m_{2tot} \left( \mathbf{a}_{B_i} + r_{i2} \ddot{\beta}_i [-\sin \beta_i \cos \beta_i]^T - r_{i2} \dot{\beta}_i^2 [\cos \beta_i \sin \beta_i]^T \right) - m_s \ddot{s}_i [\cos \beta_i \sin \beta_i]^T - 2m_s \dot{s}_i \dot{\beta}_i [-\sin(\beta_i) \cos(\beta_i)]^T \quad (14)$$

$$M_{i2} = -\ddot{\beta}_i I_{i2} - m_{2tot} r_{i2} [-\sin \beta_i \cos \beta_i] \mathbf{a}_{B_i} - 2m_s s_i \dot{s}_i \dot{\beta}_i \quad (15)$$

where  $\beta_i$ ,  $\dot{\beta}_i$  and  $\ddot{\beta}_i$  are the displacement, angular velocity and angular acceleration of the passive joints and  $m_{2tot}$  is the total mass of link  $A'_i A_i$ , that is,  $m_{2tot} = m_2 + m_s$ . Also,  $\mathbf{a}_{B_i}$  describes the linear acceleration of point  $B_i$ ,  $r_{i2}$  is the distance between the centre of mass of link  $A'_i A_i$  and point  $B_i$  while  $I_{i2}$  is the moment of inertia of the distal link with respect to  $B_i$ . The distance from point  $B_i$  to the barycentre of the redundant mass is  $s_i$  while  $\dot{s}_i$  and  $\ddot{s}_i$  describe the velocity and acceleration of  $m_s$  relative to  $B_i$ . The position of the centre of mass of the distal link and its moment of inertia vary with respect to the position of the portable mass and are written as follows:

$$r_{i2} = \frac{m_s s_i + m_2 r_{G_2}}{m_2 + m_s} \quad (16)$$

$$I_{i2} = I_{A'_i A_i} + m_s (s_i)^2 \quad (17)$$

where  $r_{G_2}$  is the position of the centre of mass of the distal link (excluding  $m_s$ ) and is equal to zero for the case when  $B_i A_i$  is equal to  $B_i A'_i$ , and  $I_{A'_i A_i}$  is the moment of inertia of link  $A'_i A_i$  about its centre of mass (excluding  $m_s$ ).

The inertial force and moment of the moving platform about point  $P$  is written as follows:

$$\mathbf{F}_N = -m_n \mathbf{a}_P \quad (18)$$

$$M_N = -\ddot{\alpha} I_N \quad (19)$$

The plots are presented in the greater scale to highlight the differences. where  $\mathbf{a}_P$  and  $\ddot{\alpha}$  are the linear acceleration of point  $P$  and the angular acceleration of the moving platform, respectively, while  $m_n$  and  $I_N$  represents the mass and the moment of inertia of the moving platform.

## 2.4. Dynamic Model

The dynamic equation of the 3-RRR is written as follows:

$$\mathbf{J}^T \boldsymbol{\tau} + \sum_{i=1}^3 \sum_{j=1}^2 [\mathbf{H}_{ij}^T \quad \mathbf{G}_{ij}^T] [\mathbf{F}_{ij} \quad \mathbf{M}_{ij}]^T [\mathbf{H}_N^T \quad \mathbf{G}_N^T] [\mathbf{F}_N \quad \mathbf{M}_N]^T = 0 \quad (20)$$

where  $\mathbf{J}$  is the Jacobian matrix of the manipulator,  $\boldsymbol{\tau}$  presents the torque vector,  $\mathbf{H}_{ij}$  are the link Jacobian sub-matrices related to velocity and  $\mathbf{G}_{ij}$  are the link Jacobian sub-matrices related to the angular velocity of the links,  $\mathbf{H}_N$  and  $\mathbf{G}_N$  represent the link Jacobian sub-matrix related to velocity and the link Jacobian sub-matrix related to the angular velocity of the moving platform,  $\mathbf{F}_{ij}$  and  $\mathbf{M}_{ij}$  are inertial forces and moments of the robot links and  $\mathbf{F}_N$  and  $\mathbf{G}_N$  represent the inertial force and moment of the moving platform.

### 3. TRAJECTORY OPTIMIZATION

When planning a trajectory in the Cartesian space, the displacement, velocity and acceleration of the end effector are known. These can be used to calculate the kinematic properties of all active joints for every point in the trajectory while the dynamic equations can be used to compute the actuator torques. Since the torques necessary to move the end effector are a function of the position, velocity and acceleration of the portable masses, moving the redundant masses (*i.e.*, changing  $s_i$ ,  $\dot{s}_i$  and  $\ddot{s}_i$  for  $i = 1, 2, 3$ ) will also have a direct effect on the torques at the base-mounted actuators.

Here, variables  $s_i$  are optimized to minimize the manipulator's total torque at a specific time step within the trajectory. The optimization problem is written as follows:

$$\min_{s_i} \sum_{i=1}^3 (\tau_i(s_i) - \lambda \bar{\tau}_i)^2 \quad (21)$$

$$\text{subject to} \quad -l_2 \leq s_i \leq l_2 \quad (22)$$

$$-\dot{s}_{\max} \leq \dot{s}_i \leq \dot{s}_{\max} \quad (23)$$

$$-\ddot{s}_{\max} \leq \ddot{s}_i \leq \ddot{s}_{\max} \quad (24)$$

where  $\tau_i$  refers to the optimized torque of actuator  $i$  at every time step,  $\bar{\tau}_i$  is the torque value obtained when a similar manipulator without internal redundancy is used and  $\lambda$  is a coefficient between 0 and 1 which makes the objective function flexible on the percentage of the optimized torque value with respect to the torques of the non-redundant manipulator. When  $\lambda$  is equal to zero, the optimization algorithm decreases the torque as much as possible. This, however, can cause problems since the velocity or acceleration limits are sometimes attained and the optimization is not efficient. The optimization variables (*i.e.*,  $s_i$ ) refer to the distance from joint  $B_i$  to the barycentre of the corresponding redundant mass. In equation (22), the value of  $s_i$  has been constrained so as to keep it within track  $A_i'A_i$ . Also, the rate of change of  $s_i$  (*i.e.*,  $\dot{s}_i$ ) is bounded in the positive and negative directions to a maximum absolute value  $\dot{s}_{\max}$  (with  $\dot{s}_{\max} > 0$ ). In addition to this, the rate of change of  $\dot{s}_i$  (*i.e.*,  $\ddot{s}_i$ ) is bounded to a maximum absolute value  $\ddot{s}_{\max}$ . These limits prevent any sudden changes in the motion of the portable masses.

When a manipulator enters rounded corners of a trajectory, the end-effector acceleration increases suddenly. This requires tremendous amounts of torque on the ground actuators. Here, the optimization algorithm is applied when the manipulator enters the rounded corners. When the end-effector exits the rounded corners (*i.e.*, the acceleration in Cartesian space turns to zero), the portable masses return to their initial positions (*i.e.*, to  $B_i$  where  $s_i = 0$ ). Otherwise, the optimization variables meet the limits (*i.e.*,  $s_i = 1$  or  $s_i = -1$ ) and makes the optimized torque greater than the non-optimized ones. A 3-4-5 polynomial is used to plan a smooth trajectory for steering the portable masses toward their initial positions. Once the portable masses arrive at the initial positions, they remain stationary until the end-effector reaches another corner. Similarly, the optimization algorithm applies as the manipulator accelerates and the portable masses return to the initial positions after the acceleration phase. ctories choosing configurations that are fa

### 4. NUMERICAL EXAMPLE

#### 4.1. Architectural Parameters and Analyzed Trajectory

The manipulator's architectural parameters for the current example are as follows: all proximal link lengths are set to 1 m (*i.e.*,  $l_1 = 1$  m for all legs). All distal link lengths are also set to 1 m (*i.e.*,  $l_2 = 1$  m for all legs) where a track has been attached to every distal link to allow the portable mass to move from  $s_i = -1$  m to 1 m. The base and moving platforms are equilateral triangles inscribed in circles of 1 m and 0.25 m in radius, respectively. The mass  $m_1$  of each of the proximal links is 1 kg while the distal links have a

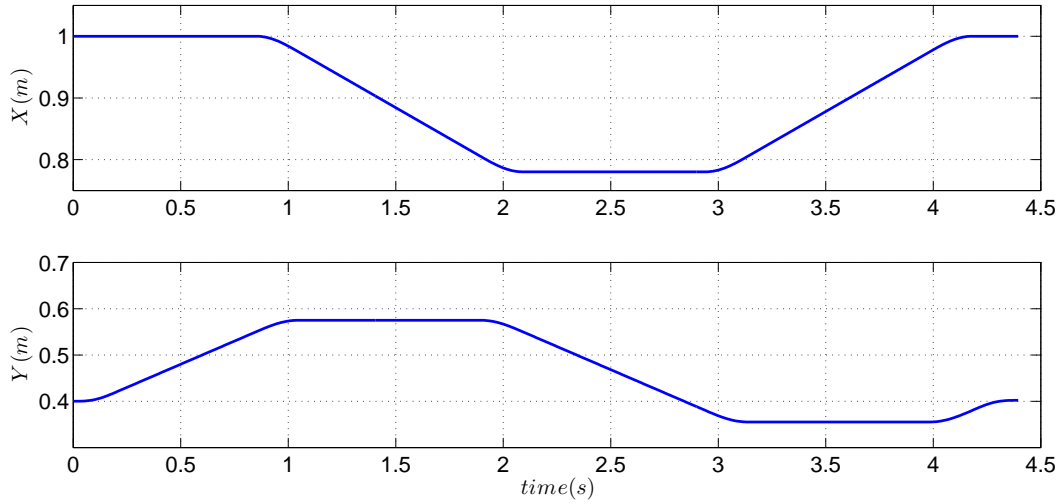


Fig. 2. Displacement of the end-effector in X and Y directions - orientation of the end-effector is constant and equal to zero along the path.

mass  $m_2 = 2$  kg (including the mass of the track) and the end effector has mass  $m_e = 0.5$  kg and the moving mass has  $m_s = 3$  kg.

#### 4.2. Trajectory Planning

The procedure has been studied on a square-shaped trajectory with rounded corners which has been planned in the Cartesian space. The end effector moves on a straight line starting from rest while keeping the end effector with constant orientation. When the tracking velocity reaches a user-defined velocity in a specified time (0.2 m/s in 0.2 s), the end effector tracks the trajectory with a constant velocity. The end effector decelerates in 0.2 s to come to a stop in the last point of the trajectory. Also,  $\delta t = 0.005$ .

The trajectory's initial position is  $p_1 = [1 \ 0.4]^T$  where the side length of the square is 0.17 m and the radius of the round corners is  $r = 0.025$  m. The trajectory starts from point  $p_1$  and goes in the positive  $Y$  direction. Once the end-effector finishes the last rounded corner, the decelerating phase commences and the end-effector stops at the point  $p_1$ . The displacement of the moving platform in both  $X$  and  $Y$  directions are presented in Fig. 2. Also, the norm of the Cartesian velocity and acceleration of the end effector are presented in Fig. 3.

The optimization problem was implemented in Matlab. The function *fmincon* was used to perform the constrained local optimization in equations (21) to (23). More particularly, the Sequential Quadratic Programming (SQP) with Hessian update option within *fmincon* was used. The SQP method is an alternative approach for handling inequality constraints in non-linear programming where SQP finds the minimum of a sequence of quadratic programming sub-problems. The objective function is estimated with a quadratic function and is minimized subject to the linearized constraints. In this method, the Hessian of the Lagrangian function is estimated at every iteration using a quasi-Newton update method. This approximation is used to create a quadratic programming sub-problem and its solution is applied to generate a search direction for the line search procedure [22]. The objective function is plotted for different iterations and the results are suggesting that the objective function is unimodal.

In the current numerical example, the velocity of the portable masses is allowed to vary in the range between  $-1$  m/s and  $+1$  m/s. The maximum absolute value of the acceleration of the portable masses is considered as  $8$  m/s<sup>2</sup> and  $m_{s_i} = 3$  kg for  $i = 1, 2, 3$ .

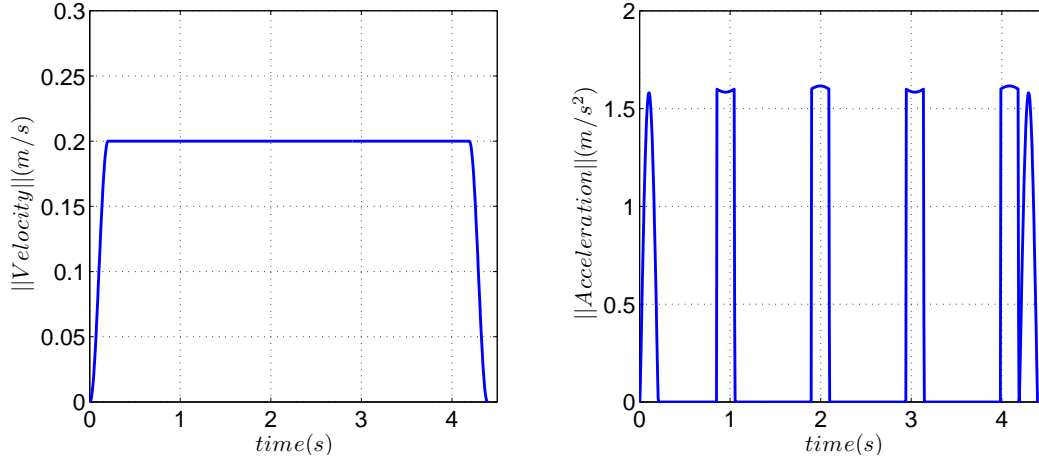


Fig. 3. Reference trajectory

The initial positions of the portable masses are chosen to be at the centre of  $A_iA'_i$  (*i.e.*,  $s_i = 0$ ) at  $t = 0$ . Thereafter, the initial position of the portable masses is considered as the solution of the optimization algorithm in the previous time step. Also, the portable masses are returned to their initial positions (centre of  $A_iA'_i$ ) after the manipulator exits a corner.

## 5. RESULTS AND DISCUSSION

Figure 4(a) illustrates the comparison between the torque values obtained from the optimization routine and the manipulator without internal redundancy (*i.e.*,  $m_{s_i} = I_{B_iA'_i} = 0$ ) for the trajectory with  $\lambda = 0.5$ . As shown in Fig. 4(a), the optimized torque is fifty percent less than the non-optimized one in both the accelerating and decelerating phases at the beginning and end of the trajectory as well as in the rounded corner areas. However, the torques of the manipulator with internal redundancy are greater than those of the non-redundant one while the end-effector acceleration is zero. When the manipulator is in the acceleration or deceleration portions at the beginning or end of the trajectory or in the rounded corner areas, the portable masses have to move in a certain direction (depending on the manipulator configuration) to provide inertial forces and moments that help to decrease the torques. Thereafter, the portable masses are moved in the opposite direction to return to their initial positions, hereafter referred to as the initialization phase, when the end-effector is not accelerating or decelerating. Consequently, the inertial forces and moments created by the motion of the portable masses in the initialization phase increase the torques at the ground joints. Also, it is noticed that the torques in the initialization phase have different values which are due to the magnitude of the velocity and acceleration of the portable masses in the initialization phase. As it is shown in Fig. 5(a), the acceleration of the portable masses 2 and 3 are greater than the acceleration of the portable mass 1 in the initialization phase at  $t = 1.1s$ . Therefore, the inertial forces and moments of the portable masses 2 and 3 are greater than the counterparts of the portable mass 1.

Figure 4(b) presents the torque of the manipulator with internal redundancy compared to the one without internal redundancy while  $\lambda = 0$ . When the objective function coefficient is equal to zero, the optimization algorithm decreases the torque as much as possible. Consequently, the portable masses need to provide greater inertial forces and moments in comparison with the former scenario (*i.e.*,  $\lambda = 0.5$ ). This leads to greater values of the velocity and acceleration in the optimization search space. As it is shown in Fig. 5(b), the accelerations of the portable masses drop to zero at several time instances (*i.e.*, the portable mass 1 at  $t = 2.11 s$ , the portable mass 2 at  $t = 0.2 s$  and the portable mass 3 at  $t = 1 s$ ) because the corresponding

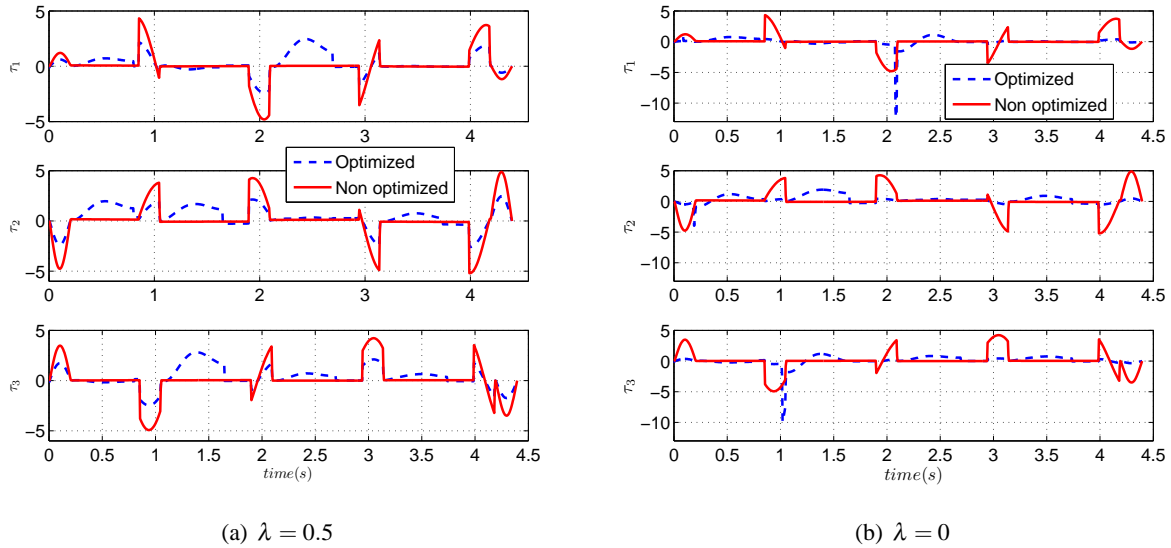


Fig. 4. The torques of the ground actuators (in N.m)

velocity meets the limit (1 m/s). The effect of  $\delta_i$  is thus eliminated from the dynamic equation. It can be seen in Fig. 4(b) that the torques of the manipulator with internal redundancy exhibit spikes at those instances and are greater than the non-redundant counterpart. It has been determined that the optimized value of the torque will be less than non-optimized one if the velocity limit of the portable mass changes to 1.2 m/s.

## 6. CONCLUSIONS

The dynamic model of a 3-RRR planar parallel manipulator involving a portable mass on the distal links is developed. The total of the squared actuator torques is investigated. An optimization algorithm is implemented to find the optimal position of the portable masses while the end effector undergoes an arbitrary trajectory with a rounded corner.

The concept was tested on a square-shaped trajectory with rounded corners. The results of the conducted test suggests that the motion of the portable masses can improve (*i.e.*, reduce) the ground actuator torques for both the accelerating and decelerating sections at the beginning and end of the trajectory. Also, the base actuator torques improve when the end effector tracks the rounded corner.

The objective function is flexible for determining the percentage of torque improvement with respect to the torque values of the same manipulator without internal redundancy. Since a higher percentage of torque improvement requires greater velocity and the acceleration limits for the portable masses, the objective function can be adjusted to keep the optimization variables within the limits.

The proposed strategy turns off the optimization algorithm when the end-effector finishes the accelerating phase and is coming out of the rounded corners areas. Then, the portable masses return to the initial positions smoothly. Therefore, the portable masses do not meet the displacement limits and the algorithm can be applied to the square-shaped trajectory with any side length. Otherwise, the portable masses may reach the displacement limits and do not have room to move further for the next rounded corner.

The obtained simulation results suggests that the application of internal redundancy in a 3-RRR planar manipulator can contribute to overcome the limits of the ground actuators (without altering the ground actuators) while the manipulator tracks a trajectory with rounded corners. This is possible as the dynamic forces required to perform the more demanding trajectories are shared by the base actuators and the additional

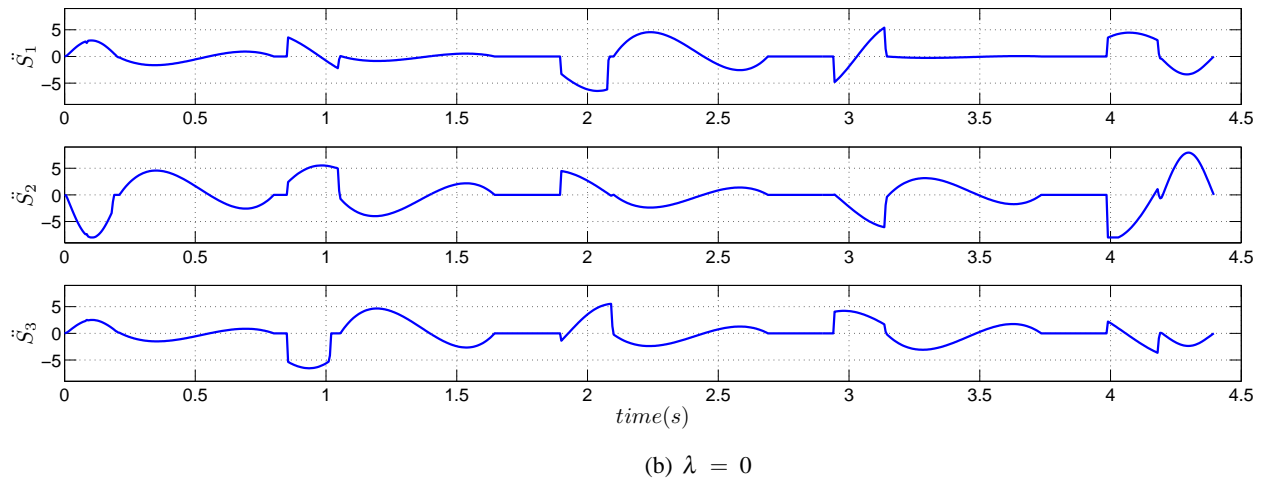
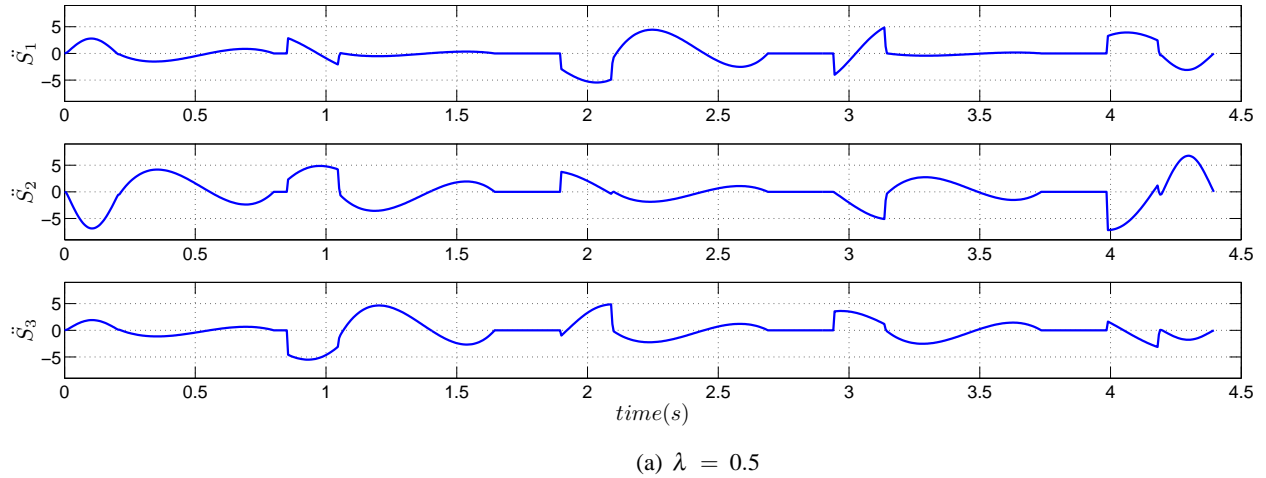


Fig. 5. Acceleration of the portable masses ( $m/s^2$ )

actuators on the distal links.

The parameters that affect the simulation are the Cartesian velocity of the end effector, the coefficient of the objective function and the allowed limits of the velocity and acceleration of the portable masses. For instance, the velocity and acceleration limits of the portable masses needs to be adjusted with respect to the dimension of the manipulator as well as the the reference trajectory. Otherwise, the velocity or acceleration of the portable masses may meet the limits and their effect will be eliminated from the dynamic equation. Moreover, due to the aforementioned force sharing effect, the balance between the contribution of the two sets of actuators to the specific task needs to be carefully considered (*e.g.*, using an objective function that considers both sets of actuators).

As future work, it is suggested to look at the trajectory globally rather than point-to-point motion planning. In that case, the position of the portable masses can be adjusted with respect to the any up-coming critical situation (*i.e.*, rounded corner).

## ACKNOWLEDGEMENTS

The authors acknowledge the financial support from the Natural Science and Engineering Research Council of Canada through their Discovery Grant program.

## REFERENCES

1. Lee, S. and Kim, S. "Kinematic analysis of generalized parallel manipulator systems." In "Proceedings of the IEEE Conference on Decision and Control," Vol. 2, pp. 1097–1102, 1993.
2. Zanganeh, K.E. and Angeles, J. "Instantaneous kinematics and design of a novel redundant parallel manipulator." In "Proceedings of IEEE Conference on Robotics and Automation," pp. 3043–3048. San Diego, USA, May 1994.
3. Merlet, J.P. "Redundant parallel manipulators." *Laboratory Robotics and Automation*, Vol. 8, No. 1, pp. 17–24, 1996.
4. Ruggiu, M. and Carretero, J.A. "Kinematic analysis of the 3-PRPR redundant planar parallel manipulator." In "Proceedings of the 2009 CCToMM Symposium on Mechanisms, Machines, and Mechatronics," Québec, Canada, May 28–29 2009.
5. Boudreau, R. and Nokleby, S. "Force optimisation of kinematically redundant planar parallel manipulators following a desired trajectory." *Mechanism and Machine Theory*, Vol. 56, pp. 138–155, 2012.
6. Cheng, H., Yiu, Y.K. and Li, Z. "Dynamics and control of redundantly actuated parallel manipulators." *IEEE/ASME Transactions on Mechatronics*, Vol. 8, No. 4, pp. 483–491. doi:10.1109/TMECH.2003.820006, December 2003.
7. Nokleby, S.B., Fisher, R., Podhorodeski, R.P. and Firmani, F. "Wrench capabilities of redundantly-actuated parallel manipulators." *Mechanism and Machine Theory*, Vol. 40, No. 5, pp. 578–599. ISSN 0094-114X, 2005.
8. Cheng, H., Liu, G.F., Yiu, Y.K., Xiong, Z.H. and Li, Z. "Advantages and dynamics of parallel manipulators with redundant actuation." In "Proceedings of the IEEE/RSJ International Conference on Intelligent Robots and Systems," pp. 171–176. Maui, USA, October 29–November 3 2011.
9. Firmani, F. and Podhorodeski, R.P. "Force-unconstrained poses for a redundantly actuated planar parallel manipulator." *Mechanism and Machine Theory*, Vol. 39, No. 5, pp. 459–476, 2004.
10. Garg, V., Carretero, J.A. and Nokleby, S.B. "A new method to determine the force and moment workspaces of actuation redundant spatial parallel manipulators." *Journal of Mechanisms and Robotics*, Vol. 1, No. 3, pp. 1–8. doi:10.1115/1.3147184, August 2009.
11. Firmani, F., Zibil, A., Nokleby, S.B. and Podhorodeski, R.P. "Force-moment capabilities of revolute-jointed planar parallel manipulators with additional actuated branches." *Transactions of the Canadian Society for Mechanical Engineering*, Vol. 31, No. 4, pp. 469–481, 2007.
12. Wang, J. and Gosselin, C.M. "Kinematic analysis and design of kinematically redundant parallel mechanisms." *Journal of Mechanical Design*, Vol. 126, No. 1, pp. 109–118, 2004.
13. Ebrahimi, I., Carretero, J.A. and Boudreau, R. "Kinematic analysis and path planning of a new kinematically redundant planar parallel manipulator." *Robotica*, Vol. 26(3), pp. 405–413, 2008.
14. Cha, S., Lasky, T.A. and Velinsky, S.A. "Kinematically-redundant variations of the 3-RRR mechanism and local optimization-based singularity avoidance." *Mechanism Based Design of Structures and Machines*, Vol. 35, pp. 15–38, 2007.
15. Wu, J., Wang, J., Wang, L. and Li, T. "Dynamic and control of a planar 3-dof parallel manipulator with actuation redundancy." *Mechanism and Machine Theory*, Vol. 44, pp. 835–849, 2009.
16. Jouaneh, K.M., Wang, Z. and Dornfeld, A.D. "Trajectory planning for coordinated motion of a robot and a position table: 1-path specification." *IEEE Transaction on Robotics and Automation*, Vol. 6, No. 6, pp. 735–745, 1990.
17. Ruggiu, M. and Carretero, J.A. "Actuation strategy based on the acceleration model for the 3-PRPR redundant planar parallel manipulator." In J. Lenarčič and M.M. Stanisic, eds., "Advances in Robot Kinematics: Analysis and Design," Springer, Piran-Portorož, Slovenia, June 27–July 1 2010.
18. Vukobratović, M., Potkonjak, V. and Matijević, V. "Internal redundancy - the way to improve robot dynamics and control performances." *Journal of Intelligent and Robotic Systems*, Vol. 27, No. 1, pp. 31–66, 2000.
19. Parsa, S.S., Carretero, J.A. and Boudreau, R. "Example of internal redundancy to improve the dynamics performance of parallel manipulators." In "Proceedings of the ASME International Design Engineering Technical

- Conferences & Mechanisms and Robotics Conference,” Chicago, Illinois, 2012.
20. Parsa, S.S., Carretero, J.A. and Boudreau, R. “A study of the effects of internal redundancy on the dynamic performance of the 3-RRR manipulator.” In “Proceeding of the 2nd IFFToMM ASIAN conference on Mechanism and Machine Science,” Tokyo, Japan, November 2012.
  21. Gosselin, C. and Angeles, J. “The optimum kinematic design of a planar three-degree-of-freedom parallel manipulator.” *Journal of Mechanism, Transmissions, and Automation in Design*, Vol. 110, pp. 35–41, 1988.
  22. Fletcher, R. *Practical Methods of Optimization*. John Wiley and Sons, 1987.